Deep learning and inverse discovery of polymer self-consistent field theory inspired by physics-informed neural networks

Danny Lin and Hsiu-Yu Yu*
Department of Chemical Engineering, National Taiwan University, Taipei 10617, Taiwan

(Received 29 April 2022; accepted 6 July 2022; published 25 July 2022)

We devise a deep learning solver inspired by physics-informed neural networks (PINNs) to tackle the polymer self-consistent field theory (SCFT) equations for one-dimensional AB-diblock copolymers. The PINNs framework comprises two parallel feedforward neural networks that separately represent the segmental partition functions and self-consistent chemical potential fields. The two networks are coupled through a loss function incorporating the governing equation, initial and boundary conditions, and the incompressibility constraint. To avoid the metastable homogeneous solution, the network parameters are initialized based on known self-consistent fields obtained from the numerical pseudospectral method. For copolymers of length N at a given volume fraction of A block (f) and the reduced Flory-Huggins interaction parameter (χN), the minimization of the loss function leads to the converged network parameters that successfully capture the stable lamellar phase. The periodicity of the lamellar structure is correctly reproduced for the explored sets of [f, χN], irrespective of the presumed computational domain size for initialization. Moreover, the proposed PINNs are applicable to the inverse discovery of the interaction parameter and the embedded chemical potential fields for an observed structure. This capability of solving the inverse SCFT problem demonstrates the potential of using PINNs to accelerate the exploration of new polymeric materials.

DOI: 10.1103/PhysRevE.106.014503

I. INTRODUCTION

In scientific and engineering problems, the embedded physical laws are often integrated through suitable governing equations with inputs representing macroscopic material properties and microscopic molecular interactions. To name just a few examples, in viscous fluids the conservation of both mass and momentum is expressed by the Navier-Stokes equations [1]. In quantum mechanics, the field solution is obtained by solving the Schrödinger equation [2]. In materials science, the phase diagram of polymeric systems is rigorously characterized using the polymer self-consistent field theory (SCFT) [3] with the fundamental equations being in the form of the modified diffusion equation. These governing equations are typically nonlinear partial differential equations (PDEs) that require substantial computational effort to meet a chosen numerical method's desired resolution and accuracy. Conventionally, the numerical process solves the equations subject to the associated conditions forwardly. The inverse prediction of physical parameters would require systematic integration of numerical solutions. Researchers are then motivated to seek for alternative paths to deal with nonlinear PDEs for complex problems with the aid of available data. Recent developments in GPU computations and machine learning techniques have significantly improved the efficiency of data operations in the fields of image recognition [4,5], natural language processing [6], and time series forecasting [7]. Distinct from the extensive data acquisition in these fields of study, physics-informed neural networks (PINNs) [8] directly incorporate relevant physical laws through nonlinear PDEs in the learning algorithm, thus significantly reducing the amount of data needed and the associated cost of data generation. In this work, we devise a PINN framework as the "deep learning solver" to tackle the phase separation of one-dimensional AB-block copolymers based on the polymer SCFT.

The polymer SCFT is a field-theoretic approach that solves the propagation equation of polymeric chains subjected to the self-consistent chemical potential field that modulates the local distribution of segments. In the mean-field fashion, this field satisfies the minimum of the free energy consisting of the configurational entropy of the Gaussian chain as well as the enthalpic interactions between different species described by the Flory-Huggins theory [9]. A modified diffusion equation governs such propagation of chains, with the natural size of the chain determining the "diffusivity" of segments. The polymer SCFT has successfully predicted the segmental distributions and morphologies of polymeric systems, including polymer brushes [10–12] and block copolymer melts [13–15], etc. Particularly, exploring the self-assembling behavior of block copolymers has been a popular research topic as the corresponding rich morphologies are suitable for various applications. Several numerical algorithms have been developed to feasibly solve the related governing equations [15–18]. However, the expensive computational cost is often unavoidable to reach the stable block copolymer structure consistent with the free energy minimum. Recently, machine learning techniques have been combined with the polymer SCFT to reproduce the phase diagram of block copolymer systems [19,20]. Making use of the free energy information from the SCFT-generated data, the monomer density field of block copolymers in one dimension has also been predicted [21]. The key ingredient

*hsiuyuyu@ntu.edu.tw

in these efforts is the employment of the known free energy components or the acquired morphologies during neural network (NN) training. In other words, the NN itself does not play a role as a solver. As an alternative, we look for a more straightforward, NN-based PDE solver that directly deals with the governing equations of the polymer SCFT.

The studies of PINNs, a deep learning framework introduced by Raissi *et al.* for solving PDEs [8], have flourished these years [22–25]. The framework utilizes a feedforward neural network (FNN) as a universal approximator [26–28] to represent the solution of a PDE. The FNN learns the network parameters by minimizing the "loss function" defined by the mean square errors of the network output subject to physically consistent constraints with input training data. In fact, this type of NN-based PDE solver was first proposed in the 1990s [29,30]. The concept has been applied previously to several physical problems, including the plasma equilibrium problem by van Milligen *et al.* [31], the N-body gravitating problem by Quito *et al.* [32], the chemical reactor problem by Parisi *et al.* [33], etc. With the current computational power that GPU offers, PINNs may deal with the involved partial derivatives efficiently through the use of the mathematical tool, automatic differentiation (AD) [34]. Therefore, researchers have the flexibility in choosing the depth (number of hidden layers) of the network and the type of the activation function without additional analytical or numerical effort in calculating the partial derivatives. PINNs have been viably extended to characterize the uncertainty of physical systems with random inputs or noisy observations [35,36], decode the governing equations by observation data such as images [37], and discovery continuum models from molecular simulations [38].

One recent employment of the NN-based PDE solver presented by Wei *et al.* [39] solves the modified diffusion equation related to the polymer SCFT equations for block copolymers. The NN solver considered there consists of two FNNs of single hidden layers. One FNN represents the segmental propagation functions, and the other represents the chemical potential fields. The network parameters are optimized by minimizing the mean square error loss defined by the conditions enforced directly by the polymer SCFT. In their implementation, the partial derivatives are handled explicitly through analytical equations, and the loss function is minimized by vanilla gradient descent. In this work, the devised PINN framework is flexible toward representing higher dimensions of parameters. To effectively initialize the network parameters toward the final solution, we utilize the chemical potential fields obtained from the numerical SCFT solutions for a given set of system-specific physical parameters as the pretraining data. The constructed NN architecture consists of a variable number of hidden layers. The involved partial derivatives are performed by AD, and the optimization is handled by a type of stochastic gradient descent, the ADAM optimizer [40]. We show that such a data-driven deep learning framework can represent the SCFT solution for specific polymer morphology (forward problem) and predict the physical parameter or chemical potential fields that lead to the desired morphology (inverse problem).

The remaining part of the paper is organized as follows. In Sec. II, we first review the general formalism and the conventional numerical procedure for solving the polymer SCFT equations. The PINN framework and the loss functions are then introduced for two systems of interest, linear homopolymers and AB-block copolymers. In Sec. III, the computational procedures for PINNs are presented in a step-by-step manner along with the associated results. The effects of the varied computational domain size are specifically compared for the copolymer systems. The application of the proposed PINN framework to both forward and inverse problems is also discussed. Finally, our findings are concluded in Sec. IV.

II. METHOD

A. Numerical self-consistent field theory approach

In the polymer SCFT, the path along the chain is characterized by the variable s that ranges from 0 to 1. The configuration of the chain is described by the partial partition functions of the fraction of segment s at position $\mathbf{r}$, $q(\mathbf{r}, s)$ and $q^\dagger(\mathbf{r}, s)$. For a polymeric chain of N segments or monomers, $q(\mathbf{r}, s)$ is the forward propagator of the first sN segments and $q^\dagger(\mathbf{r}, s)$ is the backward propagator of the remaining $(1-s)N$ segments. The chemical potential field for the species β in space, $w_\beta(\mathbf{r})$, drives the dispersion of segments in order to meet the overall free energy minimum of the system. Given $w_\beta(\mathbf{r})$, the two propagators correspond to the solutions of the modified diffusion equations,

$$\frac{\partial}{\partial s}q(\mathbf{r}, s) = \left[\frac{a^2N}{6}\nabla^2 - w_\beta(\mathbf{r})\right]q(\mathbf{r}, s), \tag{1}$$

$$\frac{\partial}{\partial s}q^\dagger(\mathbf{r}, s) = -\left[\frac{a^2N}{6}\nabla^2 - w_\beta(\mathbf{r})\right]q^\dagger(\mathbf{r}, s), \tag{2}$$

with a being the Kuhn length of the polymers. The two equations satisfy the initial conditions, $q(\mathbf{r}, 0) = q^\dagger(\mathbf{r}, 1) = 1$, and the proper periodic boundary conditions. Given the system volume V, the two propagators determine the overall partition function Q and the volume fraction of the chain (φ_β) according to the following relations,

$$Q = \int q(\mathbf{r}, s)q^\dagger(\mathbf{r}, s)d\mathbf{r} \tag{3}$$

and

$$\varphi_\beta(\mathbf{r}) = \frac{V}{Q}\int_\beta q(\mathbf{r}, s)q^\dagger(\mathbf{r}, s)ds. \tag{4}$$

In traditional numerical procedures, the set of modified diffusion equations [Eqs. (1) and (2)] are solved iteratively in order to reach the state of self-consistency. Among the well-known numerical approaches, the pseudospectral method efficiently handle the spatial variation in the Fourier space while maintaining the chain propagation in the s direction [16,17]. In the standard implementation, the potential field $w_\beta(\mathbf{r})$ is first initialized. By solving the propagators $q(\mathbf{r}, s)$ and $q^\dagger(\mathbf{r}, s)$ for the species, the volume fraction $\varphi_\beta(\mathbf{r})$ is then determined. Provided the overall incompressibility of the system,

$$\sum_\beta \varphi_\beta(\mathbf{r}) = 1, \tag{5}$$

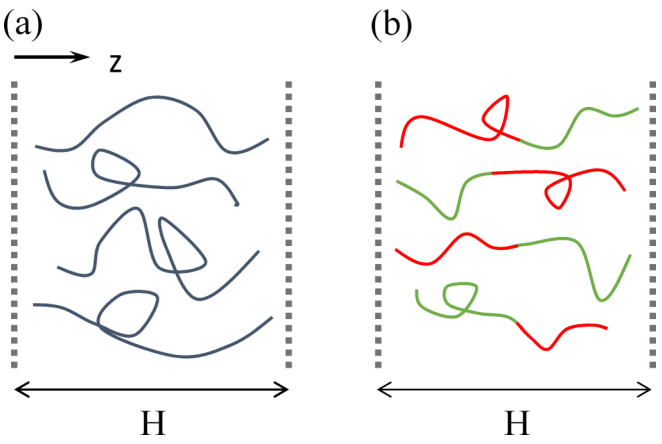

FIG. 1. The one-dimensional systems considered in this work, (a) free homopolymers and (b) AB-block copolymers. The periodic box size is H alone in the z direction.

the field is subsequently updated based on the current state of the system,

$$w_\beta(\mathbf{r}) = \sum_{\gamma\neq\beta} \chi_{\beta\gamma} N \varphi_\gamma(\mathbf{r}) + \xi(\mathbf{r}), \tag{6}$$

which corresponds to the minimum of the free energy per chain,

$$\frac{F}{k_B T} = -\ln Q + \frac{N}{2V}\sum_{\beta\gamma}\chi_{\beta\gamma}\int \varphi_\beta(\mathbf{r})\varphi_\gamma(\mathbf{r})d\mathbf{r} - \frac{1}{V} \times \sum_\beta \int w_\beta(\mathbf{r})\varphi_\beta(\mathbf{r})d\mathbf{r} - \int \xi(\mathbf{r})\left[1-\sum_\beta \varphi_\beta(\mathbf{r})\right]d\mathbf{r}, \tag{7}$$

where k_B is the Boltzmann constant, T is the temperature, β and γ represent different monomer species, $\chi_{\beta\gamma}$ is the Flory-Huggins interaction parameter between β and γ, and the spatially dependent Lagrange multiplier, $\xi(\mathbf{r})$, is introduced to enforce the incompressibility throughout the space, and is physically interpreted as the scaled pressure field. Once the field is updated, the aforementioned process is repeated until the convergence is met.

B. Physics-informed neural networks for one-dimensional self-consistent field theory

Figure 1 shows the one-dimensional systems of polymeric fluids considered, free homopolymers and AB-block copolymers. The periodic length scale is H and the unit of length is $aN^{1/2} = R_0$. In Fig. 1(a), the homopolymers consist of N segments of the same kind; in Fig. 1(b), the AB-block

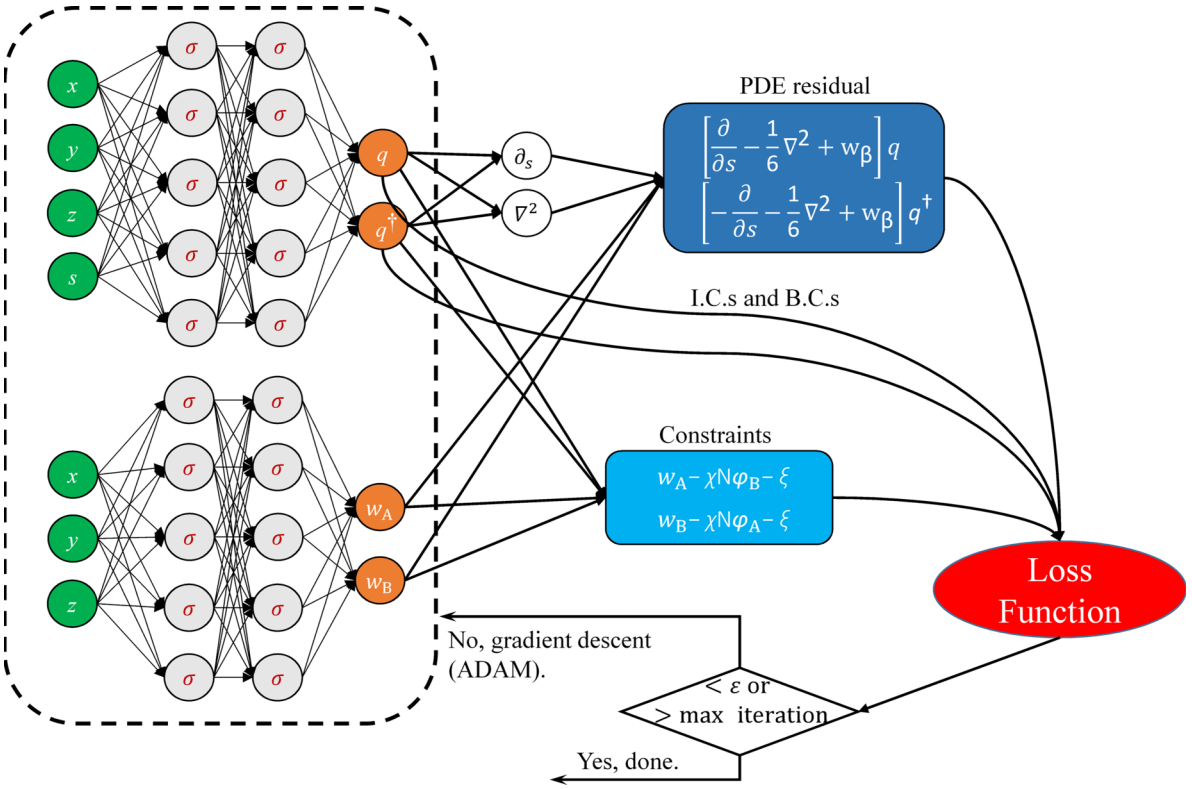

FIG. 2. The architecture of the PINN framework for solving polymer SCFT equations. This framework contains two FNNs, one representing the partition functions and the other associated with the self-consistent potential fields. σ in the hidden nodes represents the nonlinear activation function. Two networks are coupled by the loss function defined by the SCFT equations. Update of the network parameters is performed through the gradient descent algorithm generally expressed as $\Theta^{(t+1)} = \Theta^{(t)} - \eta\nabla_\Theta J(\Theta^{(t)})$, where Θ represents the parameters with the superscript t being the step index, η represents the learning rate for gradient-based updating algorithms, and $J(\Theta)$ is the total loss function (see text for definition).

copolymers are composed of covalently bonded A- and B-type homopolymers, where the first fN segments of the polymers are type A, and the remaining $(1-f)N$ segments are type B. In the mean-field fashion, the dissimilarity between the two blocks is parametrized by χN. The homopolymer system can be viewed as a special case of the block copolymer system with $\chi N = 0$.

The structure of the PINN framework for solving the polymer SCFT equations is shown in Fig. 2. The partition functions, $q(\mathbf{r}, s)$ and $q^\dagger(\mathbf{r}, s)$, accounting for the first sN segments and the remaining $(1-s)N$ segments of an N-segment polymer, are represented by the upper FNN. The chemical potential fields, $w_A(\mathbf{r})$ and $w_B(\mathbf{r})$, corresponding to the homopolymers of A type and B type are represented by the lower one. Two hidden layers are explicitly shown for clarity. The input nodes of the upper and lower FNNs are composed of variable vectors (x, y, z, s) and (x, y, z), respectively. For a given FNN of depth D, there are $D-1$ hidden layers and 1 output layer, each of which has N_h hidden nodes (neurons). In the jth hidden node of layer k with N_i input nodes from the previous layer, the nonlinear activation function, $\sigma(\tilde{z}_j^{k-1}) = \tilde{r}_j^k$ is applied to obtain the corresponding output of layer k, where $\tilde{z}_j^{k-1} = \sum_i w_{ji}^k \tilde{r}_i^{k-1} + b_j^k$ denotes the linear transformation of the output from layer $k-1$. Here, w_{ji}^k and b_j^k are the weight and bias of the neuron in layer k with $1 \leqslant j \leqslant N_h$ and $1 \leqslant i \leqslant N_i$. In the last output layer, the FNN solution is expressed as the linear combination of activations from the previous layer, $u = \sum_j v_j \sigma_j$, where v_j is the weight and u represents the NN output of q, $q^\dagger$, w_A, or w_B. These two deep FNNs are coupled by the loss function $J(\Theta)$,

$$J(\Theta) = J_{PDE}(\Theta) + J_{IC}(\Theta) + J_{BC}(\Theta) + J_C(\Theta), \tag{8}$$

where Θ is a set of trainable parameters containing all the weights and biases from both FNNs, and the terms in Eq. (8) correspond to the scaled mean-square errors of the SCFT equations and imposed conditions in the following discussion. The scaling constants (α_i, β_i and γ_i) are introduced to balance the back-propagated gradients [41].

For the one-dimensional system defined in the (z, s) space, the two modified differential equations for partition functions are written in terms of operators,

$$\hat{D}_1 q(z,s) = \left[\frac{\partial}{\partial s} - \frac{1}{6}\nabla^2 + w_\beta(z)\right] q(z,s) \tag{9}$$

and

$$\hat{D}_2 q^\dagger(z,s) = \left[-\frac{\partial}{\partial s} - \frac{1}{6}\nabla^2 + w_\beta(z)\right] q^\dagger(z,s), \tag{10}$$

respectively, where $\beta = A$ for $s \leqslant f$ and $\beta = B$ for $s > f$. The loss term for the PDE, $J_{PDE}(\Theta)$, accounts for the total residual or remainder of the PDE operators, and the data points $\{(z_r^i, s_r^i)\}_{i=1}^{N_r}$ are obtained from uniformly selecting N_r points in the z-s domain:

$$\begin{aligned} J_{PDE}(\Theta) &= \frac{\alpha_1}{2}\frac{1}{N_r}\sum_{i=1}^{N_r}\left[\hat{D}_1 q\left(z_r^i, s_r^i\right)\right]^2 + \frac{\alpha_2}{2}\frac{1}{N_r}\sum_{i=1}^{N_r}\left[\hat{D}_2 q^\dagger\left(z_r^i, s_r^i\right)\right]^2 \\ &= \frac{\alpha_1}{2}\langle[\hat{D}_1 q(z,s)]^2\rangle + \frac{\alpha_2}{2}\langle[\hat{D}_2 q^\dagger(z,s)]^2\rangle, \end{aligned} \tag{11}$$

where $\langle \ldots \rangle$ denotes the expected or mean value. On the other hand, the residuals for the two initial conditions are written as

$$\hat{B}_1 q(z,0) = q(z,0) - 1 \tag{12}$$

and

$$\hat{B}_2 q^\dagger(z,1) = q^\dagger(z,1) - 1. \tag{13}$$

The data points $\{(z_{ic}^i, 0), (z_{ic}^i, 1)\}_{i=1}^{N_{ic}}$ are sampled uniformly in $[0, H]$ and the loss term is defined as the corresponding mean-square residuals,

$$J_{IC}(\Theta) = \frac{\beta_1}{2}\langle[\hat{B}_1 q(z,0)]^2\rangle + \frac{\beta_2}{2}\langle[\hat{B}_2 q^\dagger(z,1)]^2\rangle. \tag{14}$$

The residuals for the periodic boundary conditions are expressed as

$$\hat{B}_3 q(z,s) = q(0,s) - q(H,s), \tag{15}$$

$$\hat{B}_4 q(z,s) = \frac{\partial}{\partial z}q(0,s) - \frac{\partial}{\partial z}q(H,s), \tag{16}$$

$$\hat{B}_5 q^\dagger(z,s) = q^\dagger(0,s) - q^\dagger(H,s), \tag{17}$$

$$\hat{B}_6 q^\dagger(z,s) = \frac{\partial}{\partial z}q^\dagger(0,s) - \frac{\partial}{\partial z}q^\dagger(H,s). \tag{18}$$

Similarly, the loss function is the sum of the mean-square residuals

$$\begin{aligned} J_{BC}(\Theta) = {} & \frac{\beta_3}{2}\langle[\hat{B}_3 q(z,s)]^2\rangle + \frac{\beta_4}{2}\langle[\hat{B}_4 q(z,s)]^2\rangle \\ & + \frac{\beta_5}{2}\langle[\hat{B}_5 q^\dagger(z,s)]^2\rangle + \frac{\beta_6}{2}\langle[\hat{B}_6 q^\dagger(z,s)]^2\rangle. \end{aligned} \tag{19}$$

The corresponding data points $\{(z_{bc}^i, s_{bc}^i)\}_{i=1}^{N_{bc}}$ are obtained by uniformly sampling from $s \in [0, 1]$ with z being at the boundaries. Finally, the self-consistency of the chemical potential field is imposed in the PINN in terms of the constraint operators,

$$\hat{C}_1 = w_A(z) - \chi N \varphi_B(z) - \xi(z) \tag{20}$$

and

$$\hat{C}_2 = w_B(z) - \chi N \varphi_A(z) - \xi(z), \tag{21}$$

where the volume fractions for the species A and B, φ_A and φ_B, respectively, are defined as

$$\varphi_A(z) = \frac{H}{Q_{A+B}}\int_0^f q(z,s)q^\dagger(z,s)ds \tag{22}$$

and

$$\varphi_B(z) = \frac{H}{Q_{A+B}}\int_f^1 q(z,s)q^\dagger(z,s)ds. \tag{23}$$

Q_{A+B} is the overall partition function written as

$$Q_{A+B} = \int q(z,1)dz, \tag{24}$$

and the Lagrange multiplier in Eqs. (20) and (21) satisfies

$$\xi(z) = \frac{[w_A(z) + w_B(z) - \chi N]}{2}. \tag{25}$$

The corresponding loss term is

$$J_C(\Theta) = \frac{\gamma_1}{2}\langle \hat{C}_1^2 \rangle + \frac{\gamma_2}{2}\langle \hat{C}_2^2 \rangle. \tag{26}$$

As all the data points are sampled randomly, the involved integrals are efficiently evaluated by Monte Carlo (MC) method. The computation for the overall partition function [Eq. (24)] utilizes the same dataset from the initial conditions. The data $\{z_c^i\}_{i=1}^{N_{cz}}$ are selected to evaluate the volume fractions $\varphi_A(z)$ and $\varphi_B(z)$ [Eqs. (22) and (23)]. For a given position z, separate sample points $\{s_c^i\}_{i=1}^{N_{cs}}$ are then chosen to perform the MC integration.

Unless otherwise noted, the considered PINNs consist of two FNNs with five hidden layers, each of which has 100 neurons with a hyperbolic tangent being the activation function. The loss functions are minimized by the ADAM optimizer [40], and the iteration is terminated once a prescribed maximum number of iterations is reached with a sufficiently small total loss. Distinct from traditional regression and classification problems where collecting and labeling new data is time-consuming, the generation of sample points in PINNs is straightforward with only minimal computational costs as these data points are arbitrarily selected from the domain of interest. The numbers of sample points are chosen as $N_r = 5000$, $N_{ic} = N_{bc} = 200$, N_{cz} ranges from 40 to 50, and N_{cs} ranges from 100 to 250. Two types of sampling schemes are considered during training. In the first method, the same dataset is used for the entire training process, where one "epoch" means that the model has seen all the training data points once. The second scheme generates a new dataset for each iteration where the network parameters are updated. We denote "fixed sampling" and "resampling" for the former and latter sampling schemes.

III. RESULTS AND DISCUSSION

This section presents the resulting morphologies of homopolymers and AB-block copolymers obtained from the PINN framework. The homopolymer system is chosen as a benchmark example for the NN-based SCFT solver when $\chi N = 0$. For the copolymer system, we emphasize the importance of appropriate pretraining for the network parameters and the effect of varying the periodic domain. It is anticipated that a featureless distribution function should be obtained for homopolymers, and the ordered lamellar patterns should appear for AB-clock copolymers if the Flory-Huggins interaction parameter is significant.

A. Homopolymers

Since only a single species is present, the equations for the incompressibility condition and the volume fraction [Eqs. (20) to (25)] are modified as

$$\varphi(z) = \frac{H}{Q}\int_0^1 q(z,s)q^\dagger(z,s)ds, \tag{27}$$

$$Q = \int q(z,1)dz, \tag{28}$$

and

$$\hat{C}_1 = \varphi(z) - 1. \tag{29}$$

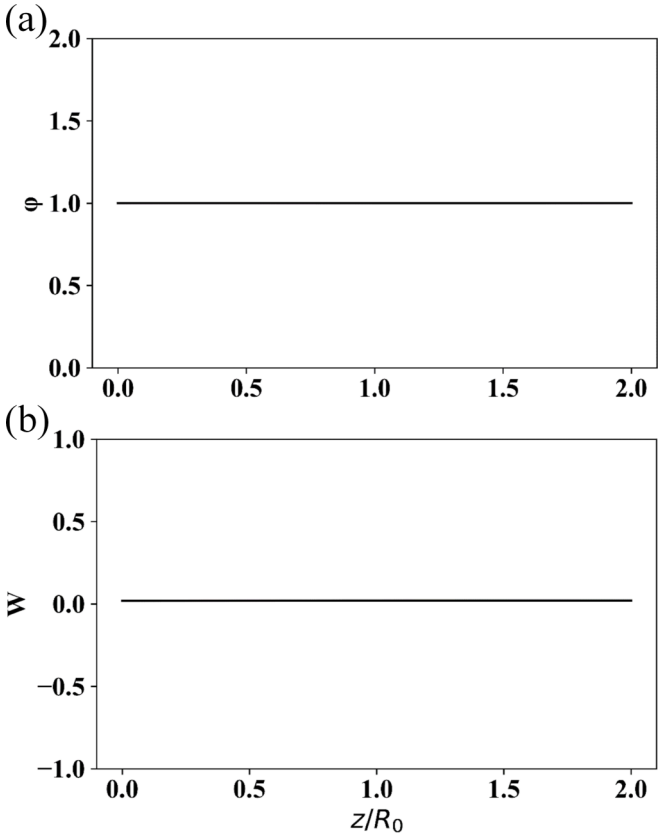

FIG. 3. Results of free homopolymers obtained from the PINN framework: (a) volume fraction distribution and (b) self-consistent field.

The fixed sampling scheme is implemented for training and $J(\Theta)$ is minimized with the hyperparameters (or scaling constants) $\alpha_1 = \alpha_2 = 1$, $\beta_1 = \beta_2 = 1000$, $\beta_3 = \beta_4 = \beta_5 = \beta_6 = 200$, and $\gamma_1 = 200$. The results after 50 000 epochs of training are shown in Fig. 3. In this benchmark test, clearly the uniform volume fraction distribution and the constant potential field for the free homopolymers are consistent with the expected state of a polymer melt.

B. AB-block copolymers

For AB-block copolymers, Eqs. (8) to (26) are taken into account in the PINN framework. The equilibrium morphology corresponding to the global free energy minimum of block copolymers is determined by the parameter set $[f, \chi N]$. In standard numerical iterations, the mean-field approximation employed in Eq. (6) gradually updates the partition functions towards the global free energy minimum. Nevertheless, the solution of the metastable disordered phase (local free energy minimum) where the volume fractions of A-block and B-block are respectively f and $(1-f)$ throughout also satisfies all the imposed conditions in the loss function for the PINN framework. As a result, random initialization of the PINN parameters easily leads to the trivial solution of a disordered phase, irrespective of the parameter set $[f, \chi N]$. In other words, naively imposing the constraints does not efficiently "teach" the PINNs to adjust the parameters to meet the global free energy minimum. To overcome this issue, we initialize

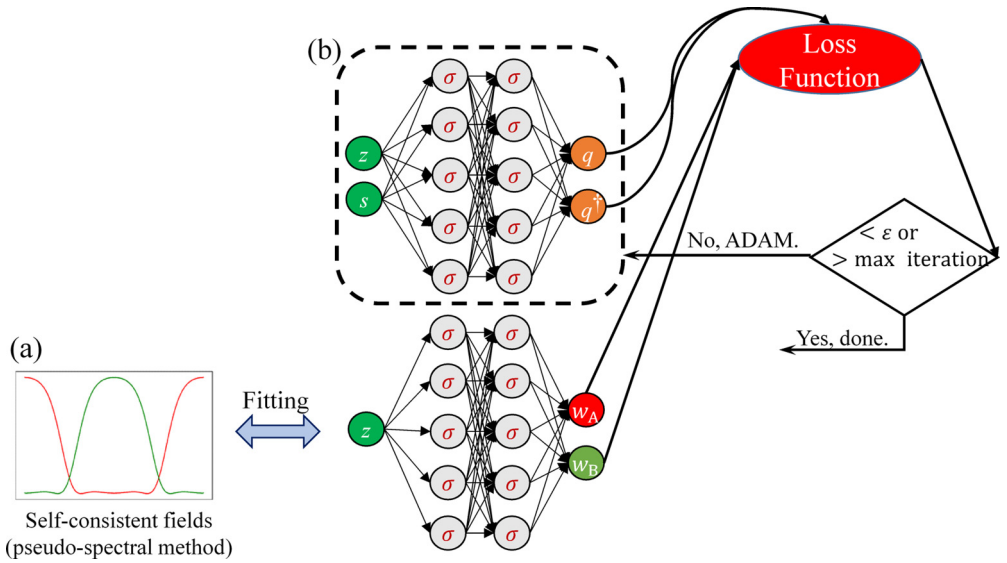

FIG. 4. Illustration of the pretraining procedure for the network parameters. (a) The lower FNN is fit with the numerical self-consistent fields obtained from the pseudospectral method. (b) The PINNs are trained with only the parameters from the upper FNN being updated.

the network parameters by pretraining techniques (scheme shown in Fig. 4) delineated as follows:

1. Forward prediction

a. Training with known fields. We utilize the self-consistent fields obtained numerically from the pseudospectral method [16,17] as the training data. For equal-block copolymers with $f = 0.5$, the onset of phase separation from a disordered phase to a lamella structure occurs at $\chi N \approx 11$, corresponding to the lamella phase with a characteristic periodic length scale of $1.35R_0$ [9]. To allow the PINNs to learn the periodicity of the morphology more easily, we first fix the computational domain as $1.35R_0$. The reference system for pretraining is selected as $[f, \chi N] = [0.5, 21]$. As presented in Fig. 5, the numerical self-consistent fields in Fig. 5(a) display periodic patterns that drive the dispersion of monomers [solid curves in Fig. 5(b)]. Therefore, a locally higher potential field for a given species generates a correspondingly higher energy barrier to overcome, leading to a lower volume fraction distribution for that species. In order for the network parameters to evolve according to the expected spatial variation in the potential fields, we first train the lower FNN for w_A and w_B with the numerical self-consistent fields by minimizing the mean-square error between the FNN output fields and the numerical fields [see Fig. 4(a) for the fitting schematic]. Once the mean-square error is sufficiently small (typically less than 10^{-3}), we start the training of PINNs by only updating the parameters of the upper FNN for the partition functions q and $q^\dagger$ [see Fig. 4(b) for the FNN enclosed in a dashed line]. In other words, the correct fields are treated as input when solving the modified diffusion equations. As the domain size is fixed as one period of the lamellar pattern, the periodic boundary conditions [Eqs. (15) to (18)] are simplified to the following Neumann form:

$$\hat{B}_7 q(z,s) = \frac{\partial}{\partial z} q(z,s), \quad z \in \partial\Omega \tag{30}$$

and

$$\hat{B}_8 q^\dagger(z,s) = \frac{\partial}{\partial z} q^\dagger(z,s), \quad z \in \partial\Omega, \tag{31}$$

where $\partial\Omega$ represents the boundary points at $z = 0$ and H. The loss function for the boundary conditions [Eq. (19)] is then replaced by

$$J_{BC}(\Theta) = \frac{\beta_7}{2}\langle[\hat{B}_7 q(z,s)]^2\rangle + \frac{\beta_8}{2}\langle[\hat{B}_8 q^\dagger(z,s)]^2\rangle. \tag{32}$$

The resampling scheme is implemented to improve the generality of network parameters. The loss function $J(\Theta)$ is minimized with $\alpha_1 = \alpha_2 = 3.2$, $\beta_1 = \beta_2 = 830$, $\beta_7 = \beta_8 = 400$, and $\gamma_1 = \gamma_2 = 265$. We define the predicted error as the mean-square error between the volume fraction profiles obtained from the pseudospectral method and the PINN prediction. In Fig. 5, the numerically obtained self-consistent fields in Fig. 5(a) are presented along with the predicted volume fraction distributions after one million iterations in Fig. 5(b) with the prediction error as small as $O(10^{-4})$. As can be seen here, the predicted volume fractions are visually indistinguishable from the pseudospectral solutions, suggesting that the PINNs can learn the correct copolymer morphology provided the correct self-consistent fields. The loss plot in Fig. 5(c) demonstrates how each loss term is optimized during the iteration process. It is shown that all the loss terms decay fairly quickly within the first 200 000 iterations.

b. Initialization with pretrained parameters. The pretrained parameters obtained from [0.5,21] are used to initialize the full PINN framework (see Fig. 2) for other sets of $[f, \chi N]$ to prevent the network parameters from being trapped in the trivial solution. In Fig. 6, we choose $[f, \chi N] = [0.5, 18]$, $[0.5, 25]$, $[0.4, 18]$, and $[0.4, 21]$ for comparison. As first seen from the pseudospectral results (solid lines), when the interaction parameter is increased at a fixed overall fraction [comparing Figs. 6(a) with 6(b) and 6(c) with 6(d)], the volume fraction profiles show broader plateaus with sharper interfaces between the AB lamellae. The sharper AB transition is accompanied by visible local variations in the

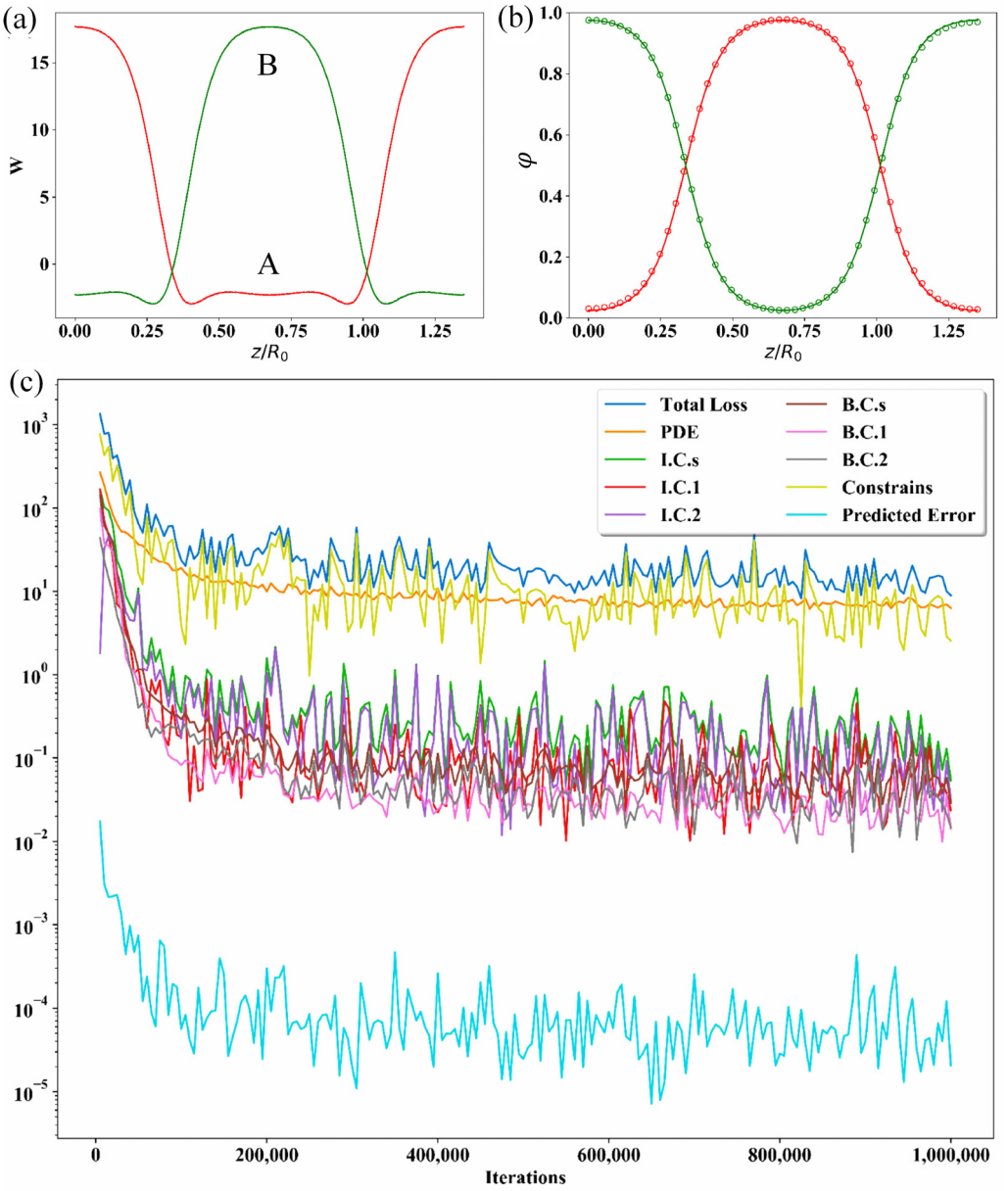

FIG. 5. Results for AB-block copolymers at $[f, \chi N] = [0.5, 21]$: (a) Input self-consistent fields, (b) volume fractions (A in red and B in green) obtained from the PINN prediction (circular markers) and the pseudospectral method (solid lines), and (c) loss plot for the PINN training.

self-consistent fields which balance the pressure field, $\xi(z)$. On the other hand, as the volume ratio changes at the fixed AB interaction [comparing Fig. 6(a) with Fig. 6(c)], the fraction of the dominant lamellar region occupied by a given species adjusts following the mass conservation.

Once the network parameters are initialized, the two FNNs are optimized with different learning rates (η_q, η_w), where η_q is the learning rate of the FNN for partition functions, and η_w is the learning rate of the FNN for self-consistent fields, respectively. A piecewise learning rate scheduler is also employed to decrease the learning rate gradually during optimization. We separately vary χN and f to compare the learning performance of the PINNs. When χN is increased at $f = 0.5$, $[\eta_q, \eta_w]$ is initially set to be $[10^{-4}, 10^{-3}]$ to allow the lower FNN for the fields to more quickly adapt to the new parameters while the upper FNN may resolve the partition functions more robustly. In contrast, as f is changed, part of the sample points originally used to represent phase A is now shifted to represent phase B. Therefore, we choose the initial learning rate for the fields to be one order of magnitude smaller than that for the partition functions, i.e., $[\eta_q, \eta_w] = [10^{-3}, 10^{-4}]$, so that the network parameters for the chemical potential fields may be slowly adjusted to the new values and the partition functions may be updated accordingly. The PINN results in Fig. 6 are presented in terms of circular symbols. As in the pretraining process, the loss function is minimized by the same set of hyperparameters, and the results are obtained from 20 000 epochs of full-batch, fixed sampling training. From the close agreement between the PINN predictions and the pseudospectral solutions, it is suggested that initialization

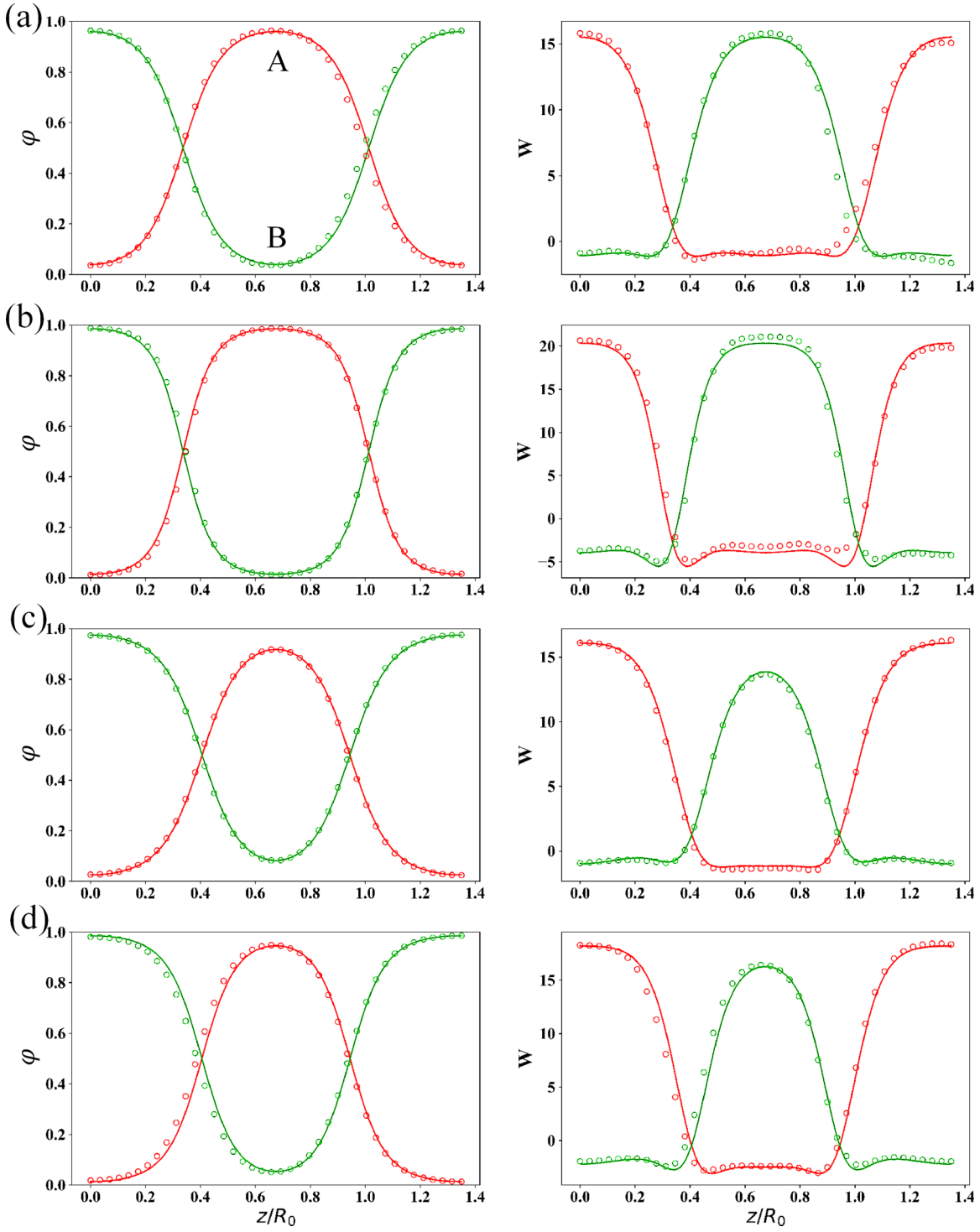

FIG. 6. Volume fraction distributions (φ) and self-consistent fields (w) of AB-block copolymers in a fixed periodic domain for $[f, \chi N]$ equal to (a) [0.5, 18], (b) [0.5, 25], (c) [0.4, 18], and (d) [0.4, 21]. The PINNs are initialized with pretrained parameters for the system of $[f, \chi N] = [0.5, 21]$ followed by a full-batch, fixed-sampling training. The PINN predictions (circular markers) are compared with the pseudospectral solutions (solid lines) for phases A (red) and B (green).

with pretrained network parameters is feasible in predicting the lamellar microstructure of diblock copolymers described by the SCFT equations in a fixed periodic domain.

c. Prediction with varied domain size. In reality, as the parameter set of $[f, \chi N]$ varies, the characteristic length scale of one period of the thermodynamically stable lamellar morphology changes accordingly to accommodate the variations in polymer fractions and interspecies affinity. Therefore, we allow the computational domain size to vary in accordance with the variation of $[f, \chi N]$ to resolve the periodic

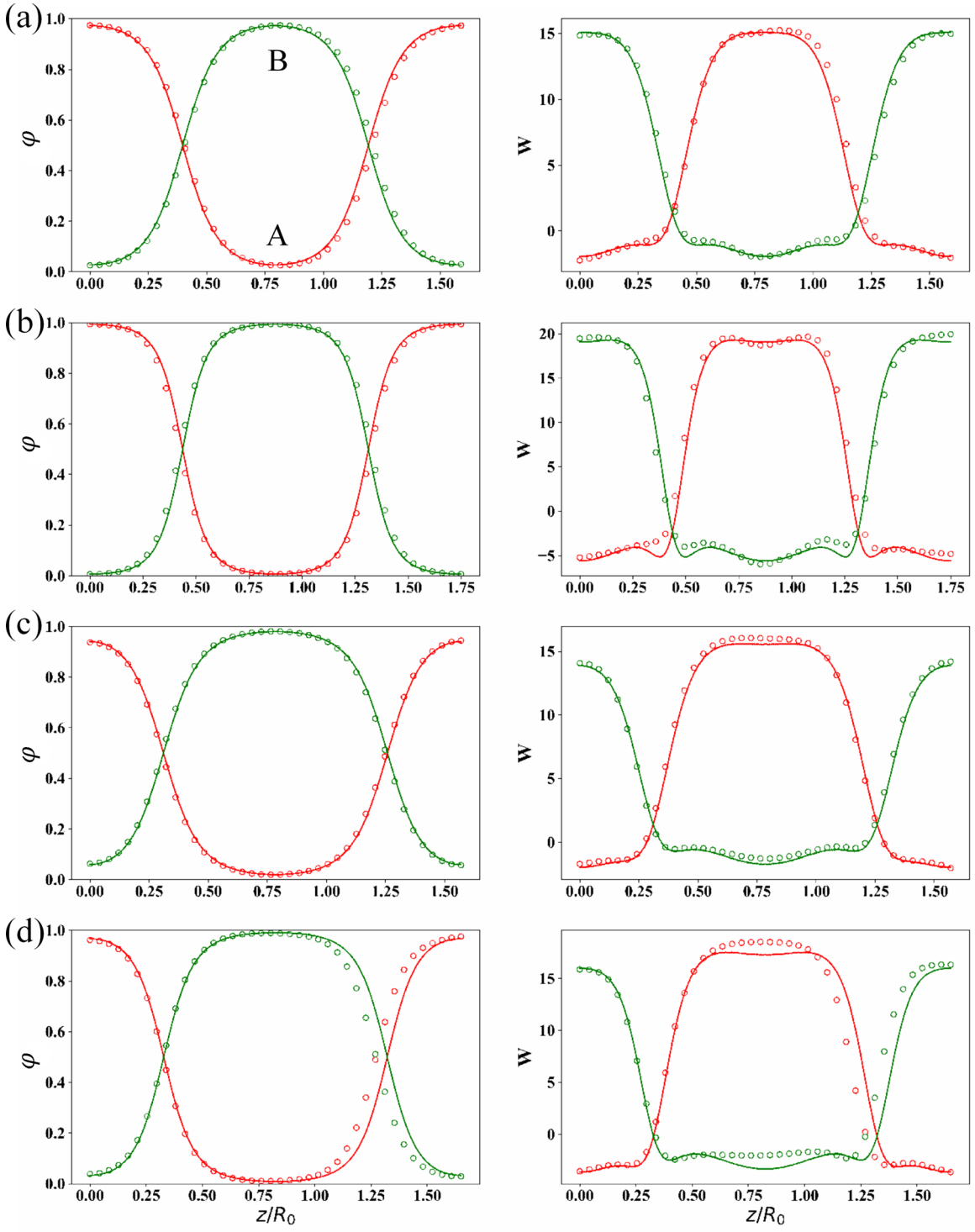

FIG. 7. Volume fraction distributions (φ) and self-consistent fields (w) of AB-block copolymers in a varied periodic domain for $[f, \chi N]$ equal to (a) [0.5, 18], (b) [0.5, 25], (c) [0.4, 18], and (d) [0.4, 21]. The PINNs are again initialized with pretrained parameters for the system of $[f, \chi N] = [0.5, 21]$ followed by a full-batch, fixed sampling training. The PINN predictions (circular markers) are compared with the pseudospectral solutions (solid lines) for phases A (red) and B (green).

microstructure corresponding to the global free energy minimum described by the polymer SCFT. In Fig. 7, the results for the same parameter sets as in Fig. 6 are compared. In general, the main characteristics of the volume fraction distributions and the self-consistent fields presented here are similar to those in Fig. 6. However, it is observed that the thermodynamically stable lamellar structure exhibits more well-defined A-rich or B-rich phases with clearer plateaus in $\varphi_A(z)$ and $\varphi_B(z)$. Consistent with the morphological changes, the corresponding variations in $w_A(z)$ and $w_B(z)$ are more substantial.

The PINN results are obtained from 200 000 epochs of full-batch, fixed sampling training for the same parameter sets

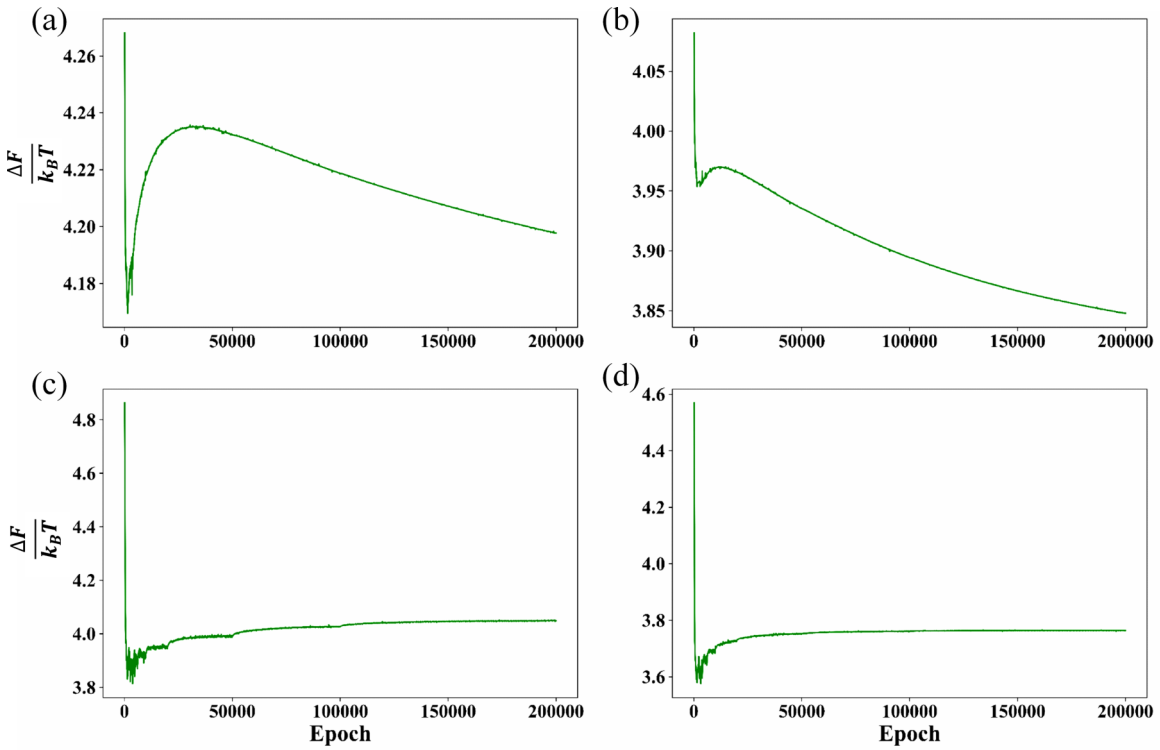

FIG. 8. The variations of free energy vs epoch for $[f, \chi N]$ equal to (a) [0.5, 21], (b) [0.5, 18], (c) [0.4, 21], and (d) [0.4, 18]. The free energy of the reference disordered state: $\frac{\Delta F}{k_B T} = \chi N f(1-f)$ is equal to (a) 5.25, (b) 4.5, (c) 5.04, and (d) 4.32.

as in Fig. 6, with the periodicity for each case been determined from the pseudospectral solutions of the SCFT equations. While there are some noticeable discrepancies between the pseudospectral results and the PINN predictions, the overall generality of the network parameters for varied periodicity is satisfactory. This suggests that pretrained parameters for one set of $[f, \chi N]$ are sufficient to properly initialize the PINNs for a different set of $[f, \chi N]$, even if the periodic spatial domain is altered. As the thermodynamically stable phase should be associated with a minimized free energy, we monitor the variation of the free energy calculated using Eq. (7) during training. Starting from the pretrained system parameter state in Sec. III B 1 a, the free energy variations for $[f, \chi N] = [0.5, 21]$, [0.5, 18], [0.4, 21], and [0.4, 18] are separately compared in Fig. 8. When $[f, \chi N]$ and the associated domain size are varied, the free energy immediately drops as the network parameters originally optimized for a smaller domain size suddenly are required to conform with the target physical state. The temporarily decreased energy does not correspond to the thermodynamically stable state, as the loss function is not yet minimized. During the training process, this disturbed free energy gradually reaches a new plateau value smaller than the reference one for the disordered state, $\frac{\Delta F}{k_B T} = \chi N f(1-f)$. This result indicates that the thermodynamic consistency is also captured during the update of the PINN parameters.

2. Inverse prediction

The examples discussed so far demonstrate the forward representation of SCFT solutions using PINNs. Nevertheless, one unique feature of the PINN framework is its capability to solve the inverse problem [8]. Once the PINNs fully represent the PDE with embedded physical laws through the trained network parameters, the inverse discovery of physical parameters or spatial fields inferred by the observations can be realized. This would be distinct from traditional numerical approaches where predictions of solutions for given parameter sets can only be achieved in a trial-and-error manner. Two scenarios that exemplify potential applications using our devised PINNs framework are considered in this section.

a. Discovery of interaction parameter. In general, a PDE can be expressed as $\frac{\partial u}{\partial s} + \hat{O}[u(z,s);\lambda] = 0$, where $\hat{O}$ is a nonlinear operator, λ is a characteristic parameter, and u represents the hidden solution. In our case, u can be q, $q^\dagger$, w_A, or w_B. By treating λ as a trainable parameter, it is possible to make the PINNs predict the value of λ that best describes a given set of observable data $\{(z_d^i, s_d^i), u_d^i\}_{i=1}^{N_{\text{Data}}}$ by minimizing the loss function with an additional loss term $J_{\text{Data}}(\Theta)$:

$$J_{\text{Data}}(\Theta) = \frac{1}{N_{\text{Data}}} \sum_{i=1}^{N_{\text{Data}}} \left[u\left(z_d^i, s_d^i\right) - u_d^i \right]^2. \tag{33}$$

Exploiting this concept, we treat the characteristic Flory-Huggins parameter χN as a trainable parameter and perform the training process with given chemical-potential fields as the training data. The objective is to obtain χN and volume fraction distributions simultaneously provided the designed self-consistent fields. Starting from the procedure of training with known fields (Sec. III B 1 a), we minimize the loss function $J(\Theta)$ with Θ containing the network parameters of the

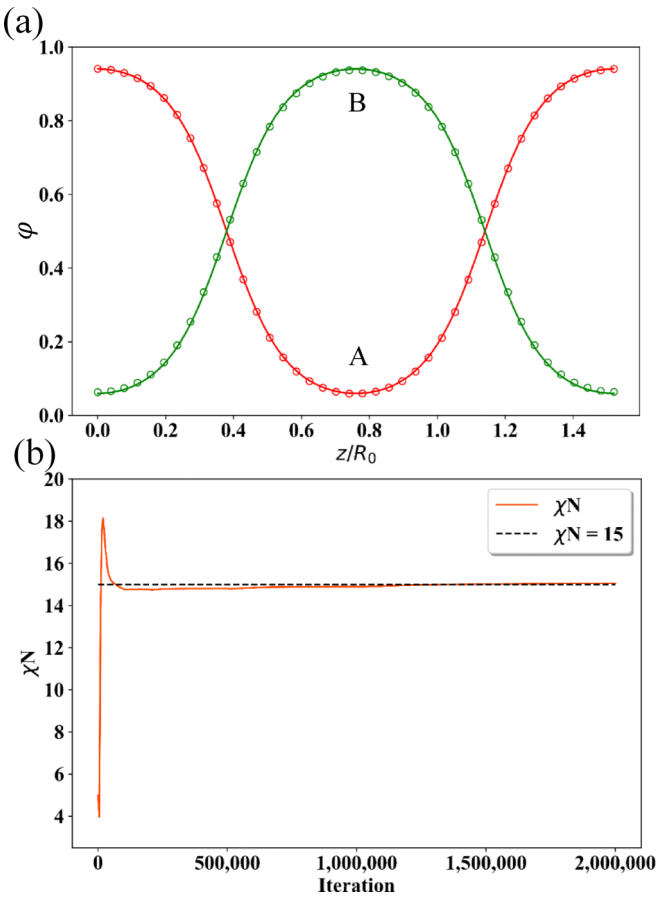

FIG. 9. Predicted results with known self-consistent fields for $[f, \chi N] = [0.5, 15]$ as the training data. (a) Volume fraction distributions, where the PINN predictions with the resampling scheme (circular markers) are compared with the pseudospectral solutions (solid lines) for A (red) and B (green). (b) Convergence of the PINN-predicted Flory-Huggins interaction parameter (solid line) compared with the actual value (dashed line).

upper FNN for the partition functions as well as χN. Treating the pseudospectral fields obtained for $[f, \chi N] = [0.5, 15]$ as the training data in $J_{\text{Data}}(\Theta)$, both the volume fraction distributions and the interaction parameter are successfully found in Fig. 9. The result suggests that the PINNs indeed "see" the parameter space in a self-consistent manner, and the correct interaction parameter is embedded in the chemical potential fields.

b. Discovery of intrinsic self-consistent fields. A more stringent test would be to consider the observed volume fraction distributions as known data and inversely predict the corresponding self-consistent fields. The training data are thus the desired copolymer volume fractions sampled at different locations, $\{z_P^i, (\varphi_{A,P}^i, \varphi_{B,P}^i)\}_{i=1}^{N_P}$. In the previous example with the data loss being defined according to Eq. (33), minimizing the data loss is done straightforwardly in terms of the actual output of the FNN. By contrast, in this case the data loss term is calculated by the mean-square error between the training data $\{\varphi_{A,P}^i, \varphi_{B,P}^i\}_{i=1}^{N_P}$ and the overall PINN predictions $\{\varphi_A(z_P^i), \varphi_B(z_P^i)\}_{i=1}^{N_P}$. The data loss term for this problem is defined as

$$J_P(\Theta) = \frac{\gamma_3}{2}\langle \hat{P}_1^2 \rangle + \frac{\gamma_4}{2}\langle \hat{P}_2^2 \rangle \tag{34}$$

with

$$\hat{P}_1 = \varphi_A(z) - \varphi_{A,P}^i(z) \tag{35}$$

and

$$\hat{P}_2 = \varphi_B(z) - \varphi_{B,P}^i(z). \tag{36}$$

The training data correspond to the integral of the FNN outputs, and the objective is to obtain the whole parameter set of the FNN for fields instead of just a single parameter. Therefore, this inverse problem is inherently more complicated. We again consider the system of $[f, \chi N] = [0.5, 15]$ to demonstrate the proposed inverse scheme. The pseudospectral volume fraction distributions are chosen as the "observable" training data. To efficiently acquire the desired training data of volume fractions from arbitrarily chosen spatial points, an extra FNN is separately introduced to fit the target volume fraction distributions by minimizing the mean-square error between its output and the pseudospectral solutions. To further ensure that the PINNs learn from the desired volume fraction

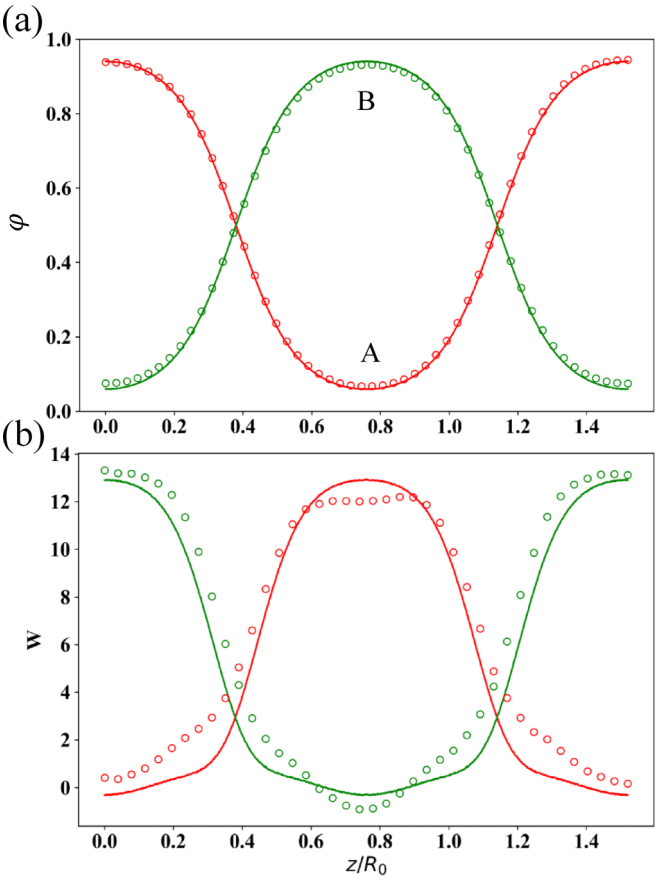

FIG. 10. Results for the inverse discovery of self-consistent morphologies with known volume fraction distributions for $[f, \chi N] = [0.5, 15]$ as the training data. (a) The PINN predictions for the volume fractions using the resampling scheme (circular markers) are compared with pseudospectral solutions (solid lines) for A (red) and B (green). (b) The corresponding results for the self-consistent fields are presented.

distributions, we constantly resample data points along the z axis to determine $\varphi_A(z)$ and $\varphi_B(z)$ in $J_C(\Theta)$ and $J_P(\Theta)$ for each iteration. In Fig. 10, the distributions and fields predicted by the PINNs with $\gamma_3 = \gamma_4 = 500$ are compared with the pseudospectral results. It can be seen that PINNs roughly capture the main characteristics of the self-consistent fields even though the networks only indirectly learn from the integral of the upper FNN for the partition functions.

Before ending this section, a few remarks regarding the inverse prediction are given. First, although χN is selected as the parameter to be discovered, in principle, other system-specific parameters can be individually or simultaneously trained in this manner provided a properly initialized PINN framework. For the discovery of self-consistent fields, it is anticipated that a given morphology such as one observed or designed experimentally can be used as the input data for PINNs to estimate the corresponding intrinsic potential fields. We have tested our framework by assigning an arbitrary volume fraction profile as the PINN input. Suppose the input morphology is inconsistent with the governing equation and/or the imposed constraints. In that case, either the resulting w_A and w_B show random profiles or the value of the loss does not decay. Therefore, if the predicted fields show irregular patterns without a well-defined periodicity or if the training loss fails to be minimized, the input volume fraction distribution may not be a solution to the specified SCFT equations. This inconsistency between the input data and the governing equations may also indicate that modifications to the governing equations should be taken action to describe the system of interest more adequately.

IV. CONCLUSIONS

In this work, the one-dimensional polymer SCFT equations were solved using the PINN framework, where the hidden solutions for PINNs include the segmental partition functions and self-consistent fields. Both the systems of linear homopolymers and AB-block copolymers were examined. We obtained the universal uniform volume fraction distribution in the test system of linear homopolymers. For AB-block copolymers of given $[f, \chi N]$ sets associated with the phase separation condition, the expected lamellar structures were forwardly predicted if the network parameters were first properly initialized through the pretraining procedure with correct self-consistent fields. We have shown that the pretraining procedure is feasible for fixed and varied computational domains. The capability of the inverse prediction using PINNs was demonstrated by two examples, where the predictions were performed on the basis of known or observable data. In the first example, given the known self-consistent fields, the reduced interaction parameter was predicted in conjunction with the lamellar volume fraction distributions. Provided the observed or desirable AB-block distributions, the key characteristics of the embedded chemical-potential fields in the system were captured in the second example.

The pretraining of network parameters employed here exemplifies the effectiveness of a good initialization. Given the available numerical solutions for polymer SCFT problems, such an initialization process can significantly reduce the convergence time. Our results also suggest that the accessible solution for one set of $[f, \chi N]$ can be practical to initialize the PINNs for systems of different parameter space. For cases where correct results are intractable to obtain beforehand, one may employ other techniques, including generating preliminary results by first solving the low-fidelity inverse problem with a small number of iterations [22]. When there are multiple free energy minimums associated with metastable solutions, the usage of adaptive activation functions and the inclusion of $L2$ regularization in the loss function may also help in avoiding spurious convergence to a local minimum [42]. With the versatility of combining with other strategies or training algorithms, once the necessary physical constraints are appropriately integrated into the loss function, the devised deep learning SCFT solver may be generalized to study the phase separation or microstructures of other block copolymer systems in multiple dimensions [13–15], polymer brushes [10–12], or more complicated polyelectrolyte systems such as polyampholytes [43,44].

The capacity to deal with inverse problems makes PINNs advantageous as PDE solvers. In contrast to numerical techniques that solve SCFT equations for known parameters and the prediction for hidden parameters can only be done in a trial-and-error manner, the inverse discovery of embedded physical parameters or potential fields presented here suggests that PINNs can be a powerful tool in material screening and the deduction of new governing equations. As elaborated in the section of discovery of self-consistent fields, our implementation shows that the thermodynamic consistency between the microstructure and potential fields is automatically encoded once the NN parameters are well-trained for the prescribed PDEs. Consequently, the PINN framework may also be iteratively trained to seek the most suitable physical constants or to determine which terms in the governing equations to keep for particular applications. Other PDEs for predicting the phase separation and the evolution of morphologies include the Cahn-Hilliard equation in the phase-field modeling [45–47]. Recent attempts have shown that machine learning algorithms can accelerate the prediction of microstructures described by the Cahn-Hilliard equation [48,49]. We, therefore, envision that the presented physics-informed framework may also be employed in the phase-field predictions by including the relevant residual terms that regularize the NN parameters to conform with the governing equations.

ACKNOWLEDGMENTS

We thank Le-Chi Lin for careful reading and valuable discussions. We acknowledge the support from the Ministry of Science and Technology in Taiwan (Grants No. MOST 105-2218-E-002-036-MY3 and No. MOST 108-2628-E-002-009-MY3) and National Taiwan University (Grants No. NTU 108L891205 and No. NTU-109L891105). We also wish to acknowledge National Center for High-Performance Computing (NCHC) for providing computational and storage resources.

[1] C. Batchelor and G. Batchelor, *An Introduction to Fluid Dynamics*, Cambridge Mathematical Library (Cambridge University Press, Cambridge, 2000).

[2] D. A. McQuarrie, *Quantum Chemistry*, 2nd ed. (University Science Books, Sausalito, 2008).

[3] G. Fredrickson, *The Equilibrium Theory of Inhomogeneous Polymers*, International Series of Monographs on Physics (Oxford University Press, Oxford, 2013).

[4] M. Pak and S. Kim, A review of deep learning in image recognition, in *Proceedings of the 2017 4th International Conference on Computer Applications and Information Processing Technology (CAIPT)* (IEEE, Piscataway, NJ, 2017), pp. 1–3.

[5] A. A. M. Al-Saffar, H. Tao, and M. A. Talab, Review of deep convolution neural network in image classification, in *Proceedings of the 2017 International Conference on Radar, Antenna, Microwave, Electronics, and Telecommunications (ICRAMET)* (IEEE, Piscataway, NJ, 2017), pp. 26–31.

[6] T. Young, D. Hazarika, S. Poria, and E. Cambria, Recent trends in deep learning based natural language processing, IEEE Comput. Intell. Mag. **13**, 55 (2018).

[7] A. Tealab, Time series forecasting using artificial neural networks methodologies: A systematic review, Future Comput. Inform. J. **3**, 334 (2018).

[8] M. Raissi, P. Perdikaris, and G. E. Karniadakis, Physics-informed neural networks: A deep learning framework for solving forward and inverse problems involving nonlinear partial differential equations, J. Comput. Phys. **378**, 686 (2019).

[9] M. W. Matsen, Self-consistent field theory and its applications, in *Soft Matter* (John Wiley & Sons, Hoboken, NJ, 2005), Chap. 2, pp. 87–178.

[10] M. W. Matsen and J. M. Gardiner, Autophobic dewetting of homopolymer on a brush and entropic attraction between opposing brushes in a homopolymer matrix, J. Chem. Phys. **115**, 2794 (2001).

[11] M. W. Matsen, Corrections to the strong-stretching theory of polymer brushes due to the entropy of the free ends, J. Chem. Phys. **117**, 2351 (2002).

[12] M. Matsen, Investigating the dominant corrections to the strong-stretching theory for dry polymeric brushes, J. Chem. Phys. **121**, 1938 (2004).

[13] M. W. Matsen and M. Schick, Stable and Unstable Phases of a Diblock Copolymer Melt, Phys. Rev. Lett. **72**, 2660 (1994).

[14] M. W. Matsen, The standard Gaussian model for block copolymer melts, J. Phys.: Condens. Matter **14**, R21 (2002).

[15] A. Arora, J. Qin, D. C. Morse, K. T. Delaney, G. H. Fredrickson, F. S. Bates, and K. D. Dorfman, Broadly accessible self-consistent field theory for block polymer materials discovery, Macromolecules **49**, 4675 (2016).

[16] K. O. Rasmussen and G. Kalosakas, Improved numerical algorithm for exploring block copolymer mesophases, J. Polym. Sci., Part B: Polym. Phys. **40**, 1777 (2002).

[17] R. B. Thompson, K. O. Rasmussen, and T. Lookman, Improved convergence in block copolymer self-consistent field theory by Anderson mixing, J. Chem. Phys. **120**, 31 (2004).

[18] G. Tzeremes, K. O. Rasmussen, T. Lookman, and A. Saxena, Efficient computation of the structural phase behavior of block copolymers, Phys. Rev. E **65**, 041806 (2002).

[19] I. Nakamura, Phase diagrams of polymer-containing liquid mixtures with a theory-embedded neural network, New J. Phys. **22**, 015001 (2020).

[20] T. Aoyagi, Deep learning model for predicting phase diagrams of block copolymers, Comput. Mater. Sci. **188**, 110224 (2021).

[21] Y. Xuan, K. T. Delaney, H. D. Ceniceros, and G. H. Fredrickson, Deep learning and self-consistent field theory: A path towards accelerating polymer phase discovery, J. Comput. Phys. **443**, 110519 (2021).

[22] G. Pang, L. Lu, and G. E. Karniadakis, fPINNs: Fractional physics-informed neural networks, SIAM J. Sci. Comput. **41**, A2603 (2019).

[23] G. E. Karniadakis, I. G. Kevrekidis, L. Lu, P. Perdikaris, S. Wang, and L. Yang, Physics-informed machine learning, Nat. Rev. Phys. **3**, 422 (2021).

[24] E. Schiassi, R. Furfaro, C. Leake, M. De Florio, H. Johnston, and D. Mortari, Extreme theory of functional connections: A fast physics-informed neural network method for solving ordinary and partial differential equations, Neurocomputing **457**, 334 (2021).

[25] S. Wang, X. Yu, and P. Perdikaris, When and why PINNs fail to train: A neural tangent kernel perspective, J. Comput. Phys. **449**, 110768 (2022).

[26] K. Hornik, M. Stinchcombe, and H. White, Multilayer feedforward networks are universal approximators, Neural Networks **2**, 359 (1989).

[27] K. Hornik, Approximation capabilities of multilayer feedforward networks, Neural Networks **4**, 251 (1991).

[28] G. Cybenko, Approximation by superpositions of a sigmoidal function, Math. Control Signals Syst. **2**, 303 (1989).

[29] M. W. M. G. Dissanayake and N. Phan-Thien, Neural-network-based approximations for solving partial differential equations, Commun. Numer. Methods Eng. **10**, 195 (1994).

[30] I. Lagaris, A. Likas, and D. Fotiadis, Artificial neural networks for solving ordinary and partial differential equations, IEEE Trans. Neural Networks **9**, 987 (1998).

[31] B. P. van Milligen, V. Tribaldos, and J. A. Jimenez, Neural Network Differential Equation and Plasma Equilibrium Solver, Phys. Rev. Lett. **75**, 3594 (1995).

[32] M. Quito Jr, C. Monterola, and C. Saloma, Solving n-Body Problems with Neural Networks, Phys. Rev. Lett. **86**, 4741 (2001).

[33] D. R. Parisi, M. C. Mariani, and M. A. Laborde, Solving differential equations with unsupervised neural networks, Chem. Eng. Process. **42**, 715 (2003).

[34] A. G. Baydin, B. A. Pearlmutter, A. A. Radul, and J. M. Siskind, Automatic differentiation in machine learning: A survey, J. Mach. Learn. Res. **18**, 1 (2018).

[35] Y. Yang and P. Perdikaris, Adversarial uncertainty quantification in physics-informed neural networks, J. Comput. Phys. **394**, 136 (2019).

[36] L. Yang, X. Meng, and G. E. Karniadakis, B-PINNs: Bayesian physics-informed neural networks for forward and inverse PDE problems with noisy data, J. Comput. Phys. **425**, 109913 (2021).

[37] M. Raissi, A. Yazdani, and G. E. Karniadakis, Hidden fluid mechanics: Learning velocity and pressure fields from flow visualizations, Science **367**, 1026 (2020).

[38] R. G. Patel, I. Manickam, N. A. Trask, M. A. Wood, M. Lee, I. Tomas, and E. C. Cyr, Thermodynamically consistent physics-informed neural networks for hyperbolic systems, J. Comput. Phys. **449**, 110754 (2022).

[39] Q. Wei, Y. Jiang, and J. Z. Y. Chen, Machine-learning solver for modified diffusion equations, Phys. Rev. E **98**, 053304 (2018).

[40] D. P. Kingma and J. Ba, Adam: A method for stochastic optimization, arXiv:1412.6980.

[41] S. Wang, Y. Teng, and P. Perdikaris, Understanding and mitigating gradient pathologies in physics-informed neural networks, SIAM J. Sci. Comput. **43**, A3055 (2021).

[42] A. D. Jagtap, K. Kawaguchi, and G. E. Karniadakis, Adaptive activation functions accelerate convergence in deep and physics-informed neural networks, J. Comput. Phys. **404**, 109136 (2020).

[43] L.-J. Qu, X. Man, C. C. Han, D. Qiu, and D. Yan, Responsive behaviors of diblock polyampholyte brushes within self-consistent field theory, J. Phys. Chem. B **116**, 743 (2012).

[44] D. L. Z. Caetano, S. J. de Carvalho, R. Metzler, and A. G. Cherstvy, Critical adsorption of periodic and random polyampholytes onto charged surfaces, Phys. Chem. Chem. Phys. **19**, 23397 (2017).

[45] G. R. Lázaro, I. Pagonabarraga, and A. Hernández-Machado, Phase-field theories for mathematical modeling of biological membranes, Chem. Phys. Lipids **185**, 46 (2015).

[46] D. R. Tree, K. T. Delaney, H. D. Ceniceros, T. Iwama, and G. H. Fredrickson, A multi-fluid model for microstructure formation in polymer membranes, Soft Matter **13**, 3013 (2017).

[47] P. K. Inguva, P. J. Walker, H. W. Yew, K. Zhu, A. J. Haslam, and O. K. Matar, Continuum-scale modelling of polymer blends using the Cahn–Hilliard equation: Transport and thermodynamics, Soft Matter **17**, 5645 (2021).

[48] D. Montes de Oca Zapiain, J. A. Stewart, and R. Dingreville, Accelerating phase-field-based microstructure evolution predictions via surrogate models trained by machine learning methods, npj Comput. Mater. **7**, 3 (2021).

[49] C. Hu, S. Martin, and R. Dingreville, Accelerating phase-field predictions via recurrent neural networks learning the microstructure evolution in latent space, Comput. Methods Appl. Mech. Eng. **397**, 115128 (2022).